Transactions of the **13th International Conference on Structural Mechanics in Reactor Technology** (SMiRT 13), Escola de Engenharia - Universidade Federal do Rio Grande do Sul, Porto Alegre, Brazil, August 13-18, 1995

Role of welding procedure and geometry in cracking of weld vicinities in stainless steel pipings of BWRs

Jansky, J., Bonn, R.
BTB Jansky GmbH, Leonberg, Germany

ABSTRACT: A theoretical/experimental study was performed in order to record the residual weld stresses in circumferential welds on austenitic piping. The results of the study are presented in the following.
With regard to the welding of circumferential welds in austenitic piping that comes into contact with reactor water, an assessment of the susceptibility to stress-corrosion cracking must be in advance address to the carbon content of the pipe materials. The sensitization period of the weld vicinities and the magnitude of residual weld stresses in the region of geometrical discontinuities of the weld contour must be taken in consideration too.
The sensitization period in the region of the root-side heat-affected zone (HAZ), which is a function of the number of passes and of the welding process, can be assumed as 80 sec. per pass for GTAW and 20 sec. per pass for manual-arc welding. This was established both experimentally.
A parameter study performed on the FE model yielded circumferentially and longitudinally oriented residual weld stresses from 140 MPa to 220 MPa that were averaged on the inside of the pipe. The stresses were averaged over a 3-mm region adjacent to the weld flank.
If the number of passes is kept as low as possible and the joins are uniformly distributed on the pipe circumference and the interpass temperature is kept at approx. 150°C, it can be expected that even V-type welds with a low sensitization period and reduced longitudinal residual stresses will be free from crack indication during the operating lifetime of BWR plants.

1 INTRODUCTION AND OBJECTIVE

The discovery of numerous circumferential cracks in the HAZ root regions of circumferential welds in titanium-stabilized, austenitic piping of BWR plants has shown that intercrystalline crack growth under operating conditions cannot be ruled out. The required coincidence of parameters permitting operation-inherent crack growth, such as

- sensitized material
- water chemistry with O_2 and H_2O_2 and
- stress as the driving force,

is known qualitatively from the relevant literature.

If one accepts the operation-inherent BWR water chemistry in the piping with water intake from the reactor pressure vessel and with a specified carbon content of the piping material, there are actually only two question complexes to explain the crack growth:

- How, during the welding of a circumferential weld, can the weld vicinities, heated to above 1100°C, of a titanium-stabilized material be sensitized for such a long time that intercrystalline crack propagation through a corrosive medium is possible in operation? How is it possible for a dwell time of several minutes in the temperature range between 500 and 800°C to occur?
- What are the stress components of the crack-driving force when the operation-inherent stresses (internal pressure and impeded expansion) in the longitudinal direction of the pipe are below the circumferential stresses from internal pressure?

These questions directed our attention to the thermal and mechanical phenomena associated with circumferential welds on austenitic piping.
The objective of this work was

- to record qualitative stress distributions in the pipe wall as a result of the production of a multi-pass weld;
- to examine the influence of
  - welding process (gas tungsten arc welding (GTAW), metal arc welding (MAW))
  - weld geometry
  - number of passes
  - interpass temperature

  on the stress level on the inside surface of the pipe;
- to record changes in the residual-stress state through the application of the operating loads (internal pressure and impeded thermal expansion);
- to determine the thermal loading of the HAZ during welding in the sensitization-relevant temperature range between 500°C and 800°C.

2 OVERVIEW OF THE WORK PERFORMED

The results presented in this paper are from the combination of elasto-plastic Finite-Element (FE) calculations and experimentally conducted temperature measurements during welding as well as residual-weld-stress measurements/deformations after the welding of the circumferential welds.
The first FE model was calculated two-dimensionally and rotation-symmetrically for the performance of the first parameter study in order to vary the pipe support, wall-thickness ratio, weld shape and interpass temperature, Appendix 1.
The calculated residual weld stresses over the wall thickness as well as the deformations (reduction of area and pipe shortening) and the sensitization period of the HAZ regions served as the basis for the specification of test weld W3. The theoretical and experimental results were compared. The comparison of the results showed that the 3D consideration of the heat source is necessary in the case of simulated welds. In addition, it became evident that the model must also take account of the local limitation of the welding heat source and its limited local effect with regard to colder regions of the entire pipe circumference. In order to satisfy this requirement, rods of varied stiffness with respect to time were positioned transversely to the weld (model N2 in Appendix 1).

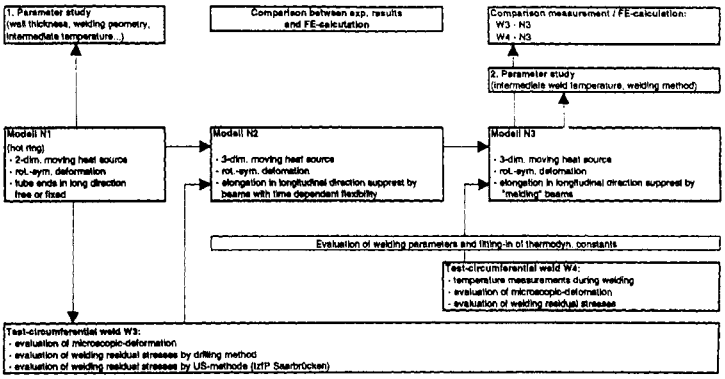

Appendix 1

The introduction of the above measures did not yield to satisfactory agreement between the numerically and experimentally determined values.
For this reason, test weld W4 with applied thermocouples was additionally performed. The measured temperature curves were compared with calculated temperature transients. It was established that the γ-δ transformation in the region of 1400°C, which was not taken into consideration in previous models, plays a not insignificant role with regard to the quantity of heat that is transmitted after fusion.
A further refinement of the theoretical deformation behaviour was achieved through the fused rods positioned parallel to the pipe segment (model N3).
This model allowed a good qualitative description and satisfactory quantitative reproduction of the experimental values. On this basis, a further parameter study was performed relating to the susceptibility of circumferential welds to stress-corrosion cracking.

3 STRUCTURE OF THE FE-MODEL

The calculation of the transient temperature fields as well as the thereon based elasto-plastic residual-weld-stress calculations were carried out using the PC version of the FE suite of programs ANSYS5.0.A /1/. Despite the use of a computer and Pentium processor, the model size had to be minimized in order for the parameter studies to be performed efficiently. The pipe geometry of the welded joint was therefore reduced to one segment, Appendix 2.

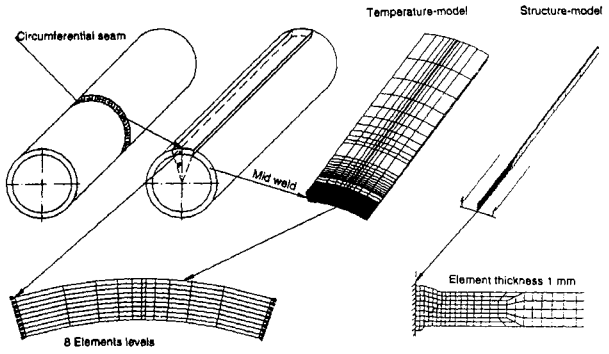

Appendix 2

Given an appropriate weld structure, use can also be made of the symmetry with respect to the centre of the weld, with only one half of the welded joint being modelled. The temperature calculation differs from the stress calculation with regard to the number of elements used in the circumferential direction of the modelled pipe

segment. Whereas a circumferential section of approx. 30° is formed by elements for the temperature calculation, the stress model comprises just one differential piece of approx. 1 mm arc length. With the large number of elements used for the temperature model in the circumferential direction and the programming of a migrating heat source, it is possible to represent the 3-dimensional thermal-conduction phenomena.
Linear 8-node volume elements were used for element formation (SOLID 70/45).
A characteristic element-edge length of 1 mm was chosen in the weld region and the adjacent HAZ. Element formation became greater with increasing distance from the centre of the weld (see Appendix 2).
The nodes at the segment edges are able to be displaced in the radial direction. By fixing these nodes in the circumferential direction the pipe geometry can be maintained. The regions of material adjacent to the structural model are taken into account by means of rod elements positioned parallel to the longitudinal axis of the pipe. The rod elements are connected to the modelled structure at a distance of 10 x wall thickness from the centre of the weld.

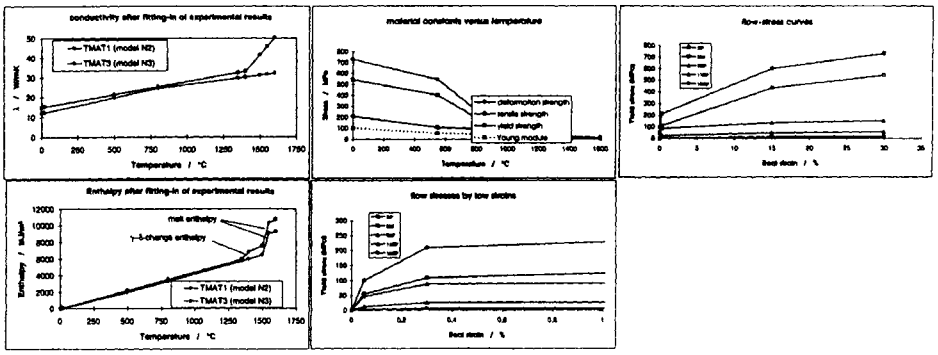

Appendix 3

The temperature-dependent material data used for the calculation is compiled in Appendix 3. The γ-δ transformation at 1400°C, which was not introduced until after experimental/theoretical comparisons, had proved to be significant with regard to the temperature analyses. The other material data was taken from the relevant literature /2, 3, 4/ and, for higher temperatures, this data was estimated according to engineering practice.
The welding heat was applied through the time-dependent specification of temperature at the node points in the respective region currently being welded.

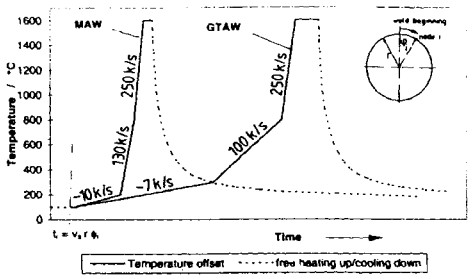

	welding velocity
welding bead 1 (GTAW)	0,37 mm/s
welding bead 2 (GTAW)	0,56 mm/s
welding bead 3 (MAW)	1,67 mm/s
welding bead 4 (MAW)	1,26 mm/s

Appendix 4

The heating temperatures and the welding speed were derived from the experimentally measured data both for GTAW and also for manual electric welding (MAW), Appendix 4.

4 WELDING EXPERIMENTS - DESCRIPTION OF SCOPE OF EXPERIMENTS

Two test welds were performed on pieces of pipe of 219.1 OD x 8 mm wall thickness made of X 6 CrNiTi 17 12 2. Test body W4 was welded with 4 passes (2 x GTAW and 2 x MAW, weaving), W3 being welded with 9 string beads (GTAW), Appendix 5. A 60° V-type weld shape was prepared in both cases.

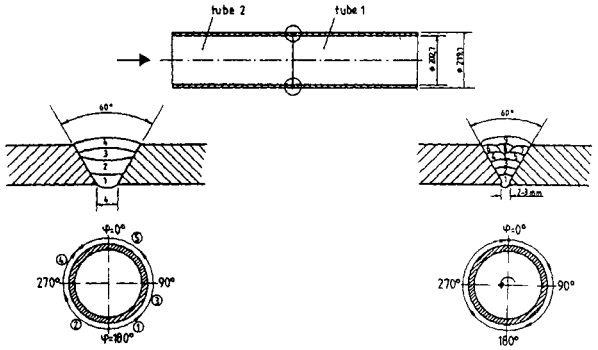

welding specification for test specimen W4	
parent material:	X 6 CrNiMoTi 17 12 2
weld geometry:	V-Naht (60°)
welding methode:	GTAW (welding bead 1 and 2) MAW (welding bead 3 and 4)
welding sequence:	comp. drawing

welding specification for test specimen W3	
parent material:	X 6 CrNiMoTi 17 12 2
weld geometry:	V-Naht (60°)
welding methode	GTAW
welding sequence	comp. drawing

Appendix 5

Test body W4 was equipped with 7 thermocouples (3 x in the circumference of the weld flank and 4 x at various distances from the weld flank). As can be seen from Appendix 6, the tips of the thermocouples were welded on at the centre of the wall thickness (blind holes). The deformations in the longitudinal and radial directions were also measured on both test bodies after welding had been completed.

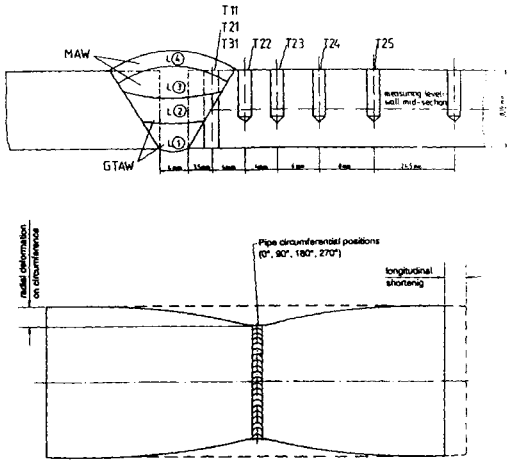

Appendix 6

The residual weld stresses were measured on test body W3 at circumferential positions 0 and 180° on both the inside and outside surfaces by means of the borehole method. For test body W4, the residual stresses were measured at circumferential position 135° on the outside. The measuring-location charts are shown in Appendix 7. The residual stresses originating from the manufacture of the pipe pieces were measured at a distance of 150 mm from the centre of the weld.

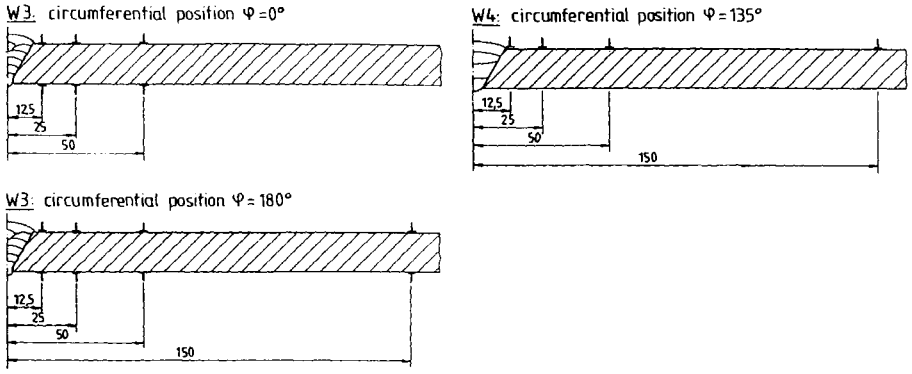

Appendix 7

5 VERIFICATION CALCULATION OF TWO CIRCUMFERENTIAL WELDS (W3 AND W4); COMPARISON WITH EXPERIMENT

The temperature curves in the vicinity of the weld flank determined in the first series of calculations were compared with the measured temperature curves. Shown by way of example in Appendix 8 are the temperature curves that were measured and calculated at a distance of 9.5 mm from the weld flank. Shown in the same appendix are the experimentally and numerically determined dwell times of the structure between 500 and 800°C. The numerically shown regions that were heated to above 500°C during welding are enclosed by solid lines. The dwell time recorded experimentally in regions T21, T31 and T22 agrees well with the numerical data. The same diagram shows the regions that experienced identical temperatures or higher than 1100°C (recrystallization). In this region, the sensitization period is approx. 230 sec.

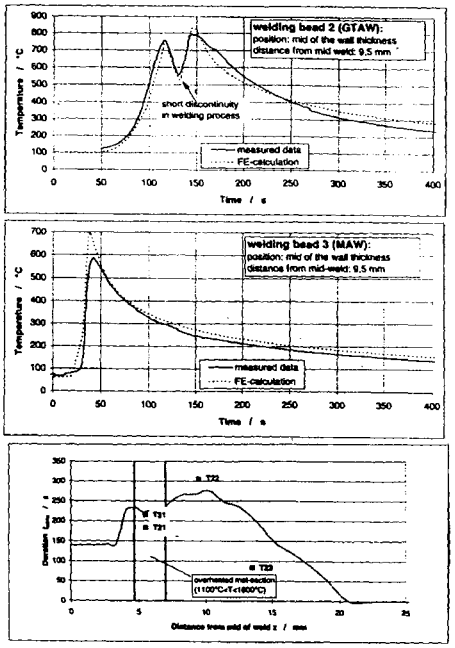

Appendix 8

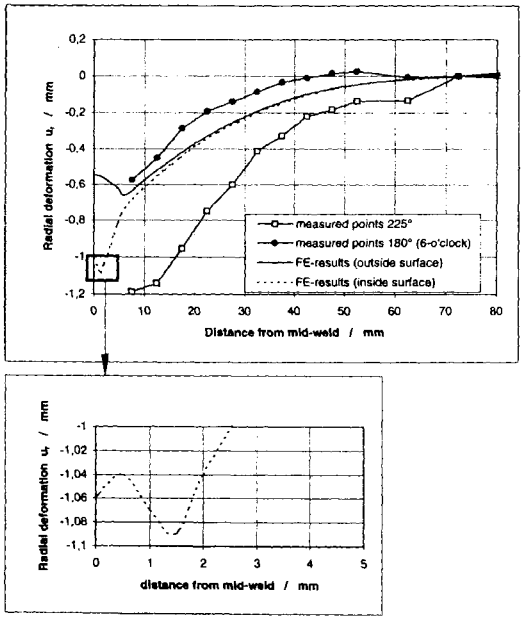

Appendix 9

The comparison between calculation and measurement for the radial reduction of area can be seen in Appendix 9 for circumferential weld W4.
The measured displacements exhibit a dependence on the circumferential position. The measured data shown here represents the maximum deviations from eight series of measurements on the pipe circumference. It can further be seen that the reduction of area occurs up to 60 mm distance from the centre of the weld. The FE deformation curve (outside) is in the centre of the experimentally measured min/max curves. The additionally shown deformation curve of the inside of the pipe exhibits an incipient crease at the transition from the root tip to the base material (see detailed picture).
The differences in the measured data on the pipe circumference point to strong local influences during welding, such as

- tacking, tack lengths
- pipe offset
- joins (beginning and end of weld)
- pauses in welding and
- possible welding defects (e.g. lack of root fusion).

These causes were observed and assessed in /5/.

Since these influences were not included in the model presented, it can be expected that there will not be satisfactory quantitative agreement for all positions on the weld circumference with regard to both the deformation values and also the stress values. Consequently, the quantitative results are only of limited indicational validity.
The stress distributions calculated for 4-pass weld W4 (2 x GTAW, 2 x MAW) are shown in Appendix 10. The here calculated longitudinal stresses have a maximum of 230 N/mm^2 next to the weld. The stresses calculated in the circumferential direction are shown as 300 N/mm^2 in the wall centre.

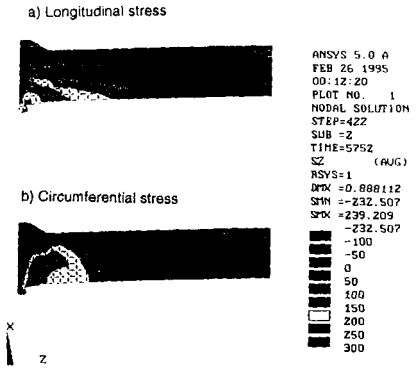

Appendix 10

The calculated stress curves and the residual stresses measured at discrete points are compared in Appendix 11. Connected in each case are the residual-stress values measured using the borehole method. The manufacture-induced residual stresses measured locally at a distance of 150 mm from the weld centre (magnitude of the yield points) were subtracted from all measured values. The cause of the manufacture-induced residual stresses may possibly be attributable to the straightening of the semi-finished products after undefined quenching in the water bath. Consequently, the shaded area represents the possible range of the residual weld stresses. This presupposes that there are the same manufacture-induced residual stresses throughout

the measured region of the pipe. That this assumption is incorrect can be deduced from the differences in measurement between W3 and W4.

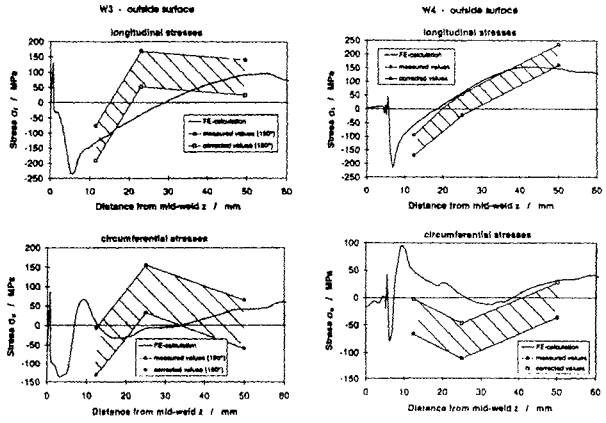

Appendix 11

The curves formed from the experimental values show good qualitative agreement with the numerically calculated stress curves. A similar tendency can also be observed in Appendix 12, which gives the residual weld stresses on the inside of the pipe.
Overall, it can be stated that the numerically calculated values show very good qualitative agreement with the experimental data. Furthermore, there was very good quantitative agreement between FE-model and experiment with regard to the temperatures.

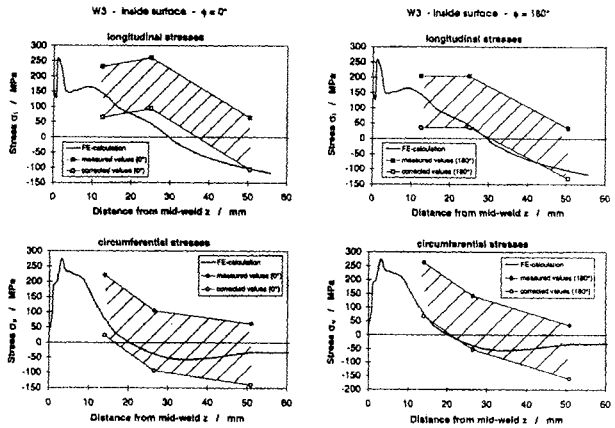

Appendix 12

Quantitative deviations between the calculated and the measured deformations could be attributed to local effects on the pipe circumference.
The quantitative differences between the calculated and the measured residual stresses are actually not surprising in view of insufficient knowledge of the manufacture-induced residual stresses. These are also potentially present in installed piping.
For these reasons, the developed and previously experimentally verified weld model was used for comparative calculations for variation of the weld parameters.

6 PARAMETER STUDY

The matrix of the study is shown in Appendix 13. Nine welds with weave beads and one weld with nine string beads were calculated and analyzed. The following were

varied: welding process (GTAW/MAW), number of passes, interpass temperature, wall-thickness ratio, weld geometry (V-60°, narrow-gap weld) and the number of fusion processes (2 for simulation of the joins on the weld circumference). In addition, a weld was performed with a ring insert in the root region.

Parameter study

Model variant	W4S1	W4S5	W4S6	W4S12	W4S9	W4S17	W4S11	W4S16	W4S13	W52S
Welding procedure	GTAW/MAW	GTAW	MAW	GTAW/MAW	GTAW/MAW	GTAW/MAW	GTAW/MAW	GTAW/MAW	GTAW/MAW	GTAW
number of weld beads	4	4	4	8	4	4	4	4	4	9
intermediate weld temperature	~ 100 °C	~ 100 °C	~ 100 °C	~ 100 °C	~ 200 °C	~ 100 °C	~ 100 °C	~ 100 °C	~ 100 °C	180 °C
wall-thickness ratio (da/di)	1,08	1,08	1,08	1,08	1,08	1,4	1,08	1,08	1,08	1,08
weld geometry	60°-V	60°-V	60°-V	60°-V	60°-V	60°-V	narrow gap welding	60°-V	60°-V	60°-V
number of melting occurancies	1	1	1	1	1	1	1	2	1	1

changed parameter

Appendix 13

Since the sensitization processes in the material are localized by the exceeding of the solubility line at approx. 1100°C, the calculated stresses for this region were averaged on the inside of the pipe. They are plotted in Appendix 14 for individual parameters. Proceeding from model experiment W4, which serves as a reference model and has been shown with longitudinal stresses of 195 N/mm^2, it can be seen that two-times fusion is capable of increasing the longitudinal stresses up to 215 N/mm^2. Above the reference weld there are further welds with an interpass temperature of 200°C as well as the narrow-gap weld.

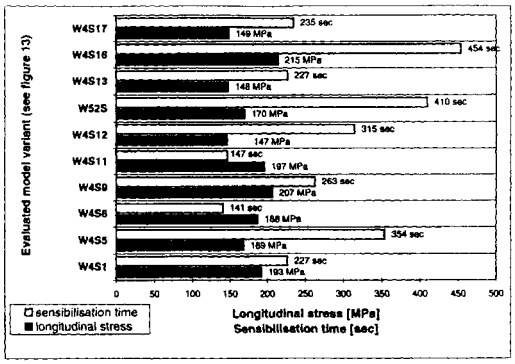

Appendix 14

Lower longitudinal stresses are achieved with 4 MAW passes and 4 GTAW passes. The 9-string-bead weld was assessed at approx. 170 N/mm^2. The low longitudinal stresses occur with 8 weave beads, the weld with ring insert in the root region and thick-walled circumferential welds. Basically, it can be stated that thin root passes with subsequent thicker filler passes also cause lower longitudinal stresses on the inside of the pipe. The parameter study showed that the variation of the parameters has an influence on the calculated longitudinal stresses only within a small range extending from approx. 150 N/mm^2 to 220 N/mm^2 ($\Delta\sigma$ = 70 N/mm^2).

The evaluation of the sensitization period in the region of the base-material regions adjacent to the root is also entered for the varied parameters. At approx. 400 sec., the 9-string-bead weld is the highest. The lowest sensitization period is achieved with the narrow-gap weld and the 4 MAW passes (approx. 140 sec.). The weld joins would lead to a doubling of the times given here.

If more passes are welded than in the present paper (or if grinding-out is performed frequently during welding), it is readily possible to reach a time span of 1,800 sec. in

which a temperature of between 500 and 800°C occurs (in micrographs of the defective circumferential welds available to BTB, up to 25 passes were counted in an 8-mm wall /10/).
Superimposed operational stresses to calculated residuals stresses yield to plastification in the affected cross section. The plastification of material provide a shift of residual stress peaks from melting line to parent material, Appendix 15.

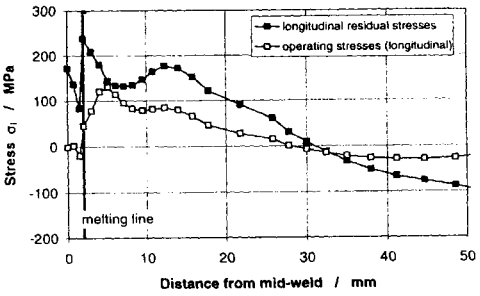

Appendix 15

7 CRACK PROPAGATION CALCULATIONS WITH DETERMINED RESIDUAL STRESSES

The crack propagations established in a pressurized-water lines in a BWR (tubes: outside diameter 216 mm x 8,5 mm , elbows: outside diameter 217,2 mm x 11,1 mm) plant can be seen in tabular form in Appendix 16. For this purpose, the operating stresses from internal pressure and thermal expansion were determined in individual cross sections. The residual weld stresses determined in the present paper for the 9-pass bead weld were superposed for the calculation of crack propagation /11/.
It can be seen that the stress magnitudes calculated in individual cross sections vary only insignificantly both with regard to the maximum and also over the wall thickness. For this reason, the crack-growth curve was varied such that the crack depths found to be destructive were reached after 15 operating years. The variation of the crack-growth curves, Appendix 17, shows approx. 1.5 decades differenz in rate of growth mm/sec. It can be concluded herefrom that it is principally the sensitization of the base-material regions that influences the rate of crack growth. Consequently, it would be expected that the parameters that lead to the minimization of the sensitization period are the decisive parameters with regard to the prevention of stress-corrosion cracking.

Findings	Crack Depth after 16 Years [mm]	Long. Stress from Internal Pressure + Bending Moment [N/mm²]
1	11	54.78
2	1.1	52.61
3	5.65	75.97
4	9.5	75.97
5	3.3	57.82
6	2.3	51.75

Bead no	Weld Residual Stresses [N/mm²]	Averaged Residual Stresses [N/mm²]
1	239	239
2	166	202.5
3	72	159
4	65	135.5
5	-15	105.4
6	-58	78.2
7	-76	56.1
8	-42	43.9
9	-7	38.2

Calculated Incubation Time [Years]	Calculated Crack Extension Parameters C	m
2.5	2,01 x 10-11	2.4
3.25	7,4 x 10-11	1.45
3.5	1,05 x 10-11	2.5
3.25	1 x 10-11	2.6
2	7 x 10-11	1.7
2.25	8 x 10-11	1.6

Appendix 16

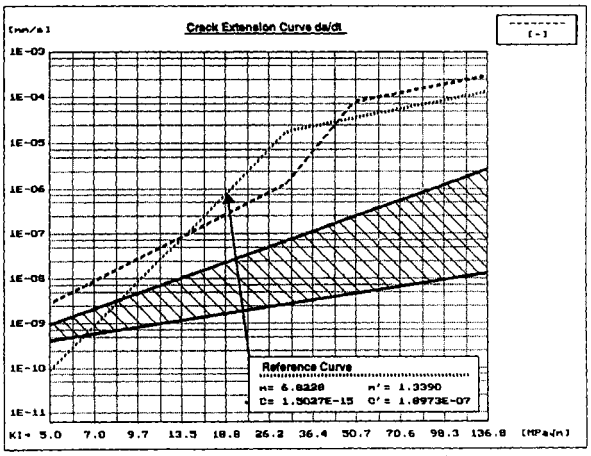

Appendix 17

8 CONCLUSIONS

The results of the present paper have shown that the magnitude of the residual weld stresses occurring in the sensitized region of material next to the fusion line on the inside of the pipe can be influenced by the choice of

- weld shape (V-type weld, narrow-gap weld)
- variation of the welding processes
- variation of the number of weld passes
- lowering of the interpass temperature
- minimization of weld joins on pipe circumference.

The highest sensitization period resulted for the 9-pass string-bead weld with 400 sec. In the extreme case of bead joins in the same circumferential position in all passes, there would be a sensitization period of 800 sec. It goes without saying that an attempt must first be made, through a reduction in the carbon content of the pipe material, to push the sensitization period into times of more than 800 sec.

A lowering of the sensitization period, thicker-walled pipes or a ring insert in the root region would result in the regions of the joins in a sensitization period of up to 440 sec. (greater distance from the 800-sec. sensitization period). The narrow-gap weld is below the thick-walled V-type weld in terms of sensitization period.

In view of the results, it can be concluded that optimally welded V-type welds will remain crack-free throughout the operating life time of a BWR. For this purpose, however, the herein established parameters should be complied with through suitable quality-assurance measures.

9 REFERENCES

/1/ "ANSYS User Manual for Revision 5.0 (Vol. 1-4)"Swanson Analysis Systems, Dezember 1992

/2/ Mannesmann Werkstoffblätter Reihe 600

/3/ Bonn, R.; "Temperaturfeldanalyse zum Schweißen von ferritischem Schweißgut auf einen austenitischen rohrförmigen Anfahrkörper" Diplom-Arbeit, Universität Stuttgart, 1993
/4/ Speidel, M.; "Gutachten zur Klärung der Ursache der Schäden an den austenitischen Rohrleitungssträngen der TC- und TD-Systeme im Kernkraftwerk Brunsbüttel", Zwischenbericht, Juni 1993
/5/ Bonn, R.; "Ergebnisse der Temperatur-, Verformungs- und Eigenspannungsmessungen an dem Versuchsrohr W4" BTB-Jansky GmbH Bericht Nr. 572, Februar 1995
/6/ Bonn, R.; "Numerische Untersuchung der Einflußgrößen auf die Schweißeigenspannungsverteilung im Bereich der Rundnähte an austenitischen Rohren" BTB-Jansky GmbH Bericht Nr. 497 Rev. A, April 1994
/7/ Bonn R.; "Der Einfluß der Zwischenlagentemperatur auf die Schweißeigenspannungsverteilung in der Umgebung von Rundnähten in dünnwandigen austenitischen Rohrleitungen" BTB-Jansky GmbH Bericht Nr. 493, Dezember 1993
/8/ Bonn, R.; "Ergebnisse der experimentellen und numerischen Untersuchungen zur Ermittlung der Schweißeigenspannungen an dem austenitischen Versuchsrohr W3" BTB-Jansky GmbH Bericht Nr. 569, November 1994
/9/ Bonn, R.; Streit, M.; "Abschlußbericht zur numerischen Simulation von Mehrlagen-Rundnähten an austenitischen Rohrleitungen" BTB-Jansky GmbH Bericht Nr. 586, Februar 1995
/10/ Listl, H.; Grafische Wiedergabe des Lagenaufbaus von Schweißnähten der Kernkraftwerke KKB, KKI-1 und KKP-1 BTB-Jansky GmbH Aktennotiz vom 05.04.1994
/11/ Jansky, J.; Andrä T.; New method for ensuring safety and availability pf pressure retaining components / PVP-Vol. 219, Transient Thermal-Hydraulics and Coupled Vessel and Piping System Responses / ASME 1991

10 Overview of Appendices

Appendix 1: Overview of studies performed
Appendix 2: Representation of weld and pipe geometry in FE model used
Appendix 3: Material data used
Appendix 4: Heating curves assumed in the FE model (according to experiment W3)
Appendix 5: Specification of welds W3 and W4
Appendix 6: Measuring-location charts of temperature and deformation measurements on welded pipes
Appendix 7: Measurement-location charts of residual weld stresses
Appendix 8: Comparison between measured and calculated temperatures (TIG and manual-arc pass)
Appendix 9: Comparison between measured and calculated radial displacements
Appendix 10: Calculated circumferential and longitudinal residual stresses in simulated W4 circumferential weld
Appendix 11: Comparison of experimental and FE results for outside surfaces W3 and W4
Appendix 12: Comparison between experimentally and numerically determined residual stresses on inside surface of pipe W3
Appendix 13: Matrix of parameter study performed
Appendix 14: Results of parameter study with regard to calculated longitudinal residual stresses and sensitization period
Appendix 15: Change of stress in longitudinal direction of pipe during service loading
Appendix 16: Calculated crack extension period
Appendix 17: Crack Extension Curves da/dt